The Cretaceous and Cenozoic tectonic evolution of Southeast Asia

Sabin Zahirovic, Maria Seton and R. Dietmar Müller

Appendix A

Table A1. The tectonic evolution of each region is based on a synthesis of a number of datasets, models and previous interpretations that are outlined below.

Region	Constraints	References
Sundaland	Basin evolution	Doust and Sumner (2007)
Luconia	Seismic sections	Clift et al. (2008)
	Continuity with Reed Bank and collision timing on Borneo/Palawan, along with cessation of subduction	Yumul Jr et al. (2003), Hutchison (2004)
(Proto) South China Sea and Semitau	Paleobiology	This study
	Sutures and ophiolites	Hutchison (1975), Metcalfe (1999)
	Gravity anomalies	This study
	Tectonic subsidence	Lin et al. (2003), Yang et al. (2004)
	Previous models	Sarewitz and Karig (1986), Briais et al. (1993)
Northern Borneo	Sutures and ophiolites	Hutchison (1975)
Central Borneo	Granitoids	Kirk (1968), Haile and Bignell (1971), Haile et al. (1977), Bignell (1972)
	Volcanics	Soeria-Atmadja et al. (1999)
Java	Metamorphics	Parkinson et al. (1998), Wakita (2000)
	Sutures and ophiolites	Hutchison (1975)
West Sulawesi	Basalts	Polvé et al. (1997)
	Metamorphics	Parkinson et al. (1998), Wakita (2000)
Luzon and Mindoro	Sutures and ophiolites	Hutchison (1975)
	Sedimentary and metamorphic basement ages	Sarewitz and Karig (1986), Encarnación (2004), Yumul et al. (2009)
East/West Philippine Arc	Sutures and ophiolites	Hutchison (1975), Yumul Jr et al. (2003), Encarnación (2004), Pubellier et al. (2004)
	Philippine Fault	Barrier et al. (1991)
	Subduction histories	Honza and Fujioka (2004), Queano et al. (2007)

Halmahera	Ophiolites	Hall et al. (1995b)
Sepik	Sutures and ophiolites	Hutchison (1975)
	Denudation histories	Crowhurst et al. (1996)
Prince Alexander, Bewani, Finisterre and Torricelli terranes	Sutures and ophiolites	Baldwin et al. (2012)
	Volcanic histories	Cullen and Pigott (1989), Klootwijk et al. (2003), Baldwin et al. (2012)
	Denudation and accretion histories	Abbott et al. (1994)
	Seismic tomography	This study
India and Kohistan-Ladakh	Sutures and ophiolites	Yin and Harrison (2000), Styron et al. (2010), Hébert et al. (2012)
	Volcanics	Chung et al. (2005), Bouilhol et al. (2013)
	India-Eurasia convergence rates	Zahirovic et al. (2012)
Burma, Sumatra and Woyla	Sutures and ophiolites	Hutchison (1975)
	Sedimentary nappes	Wajzer et al. (1991), Barber (2000), Barber and Crow (2003), Barber and Crow (2009)
Northern Gondwana	Late Jurassic syn-rift sediments	Wakita (2000)
	Oldest seafloor ages	Gradstein and Ludden (1992), Gibbons et al. (2012)

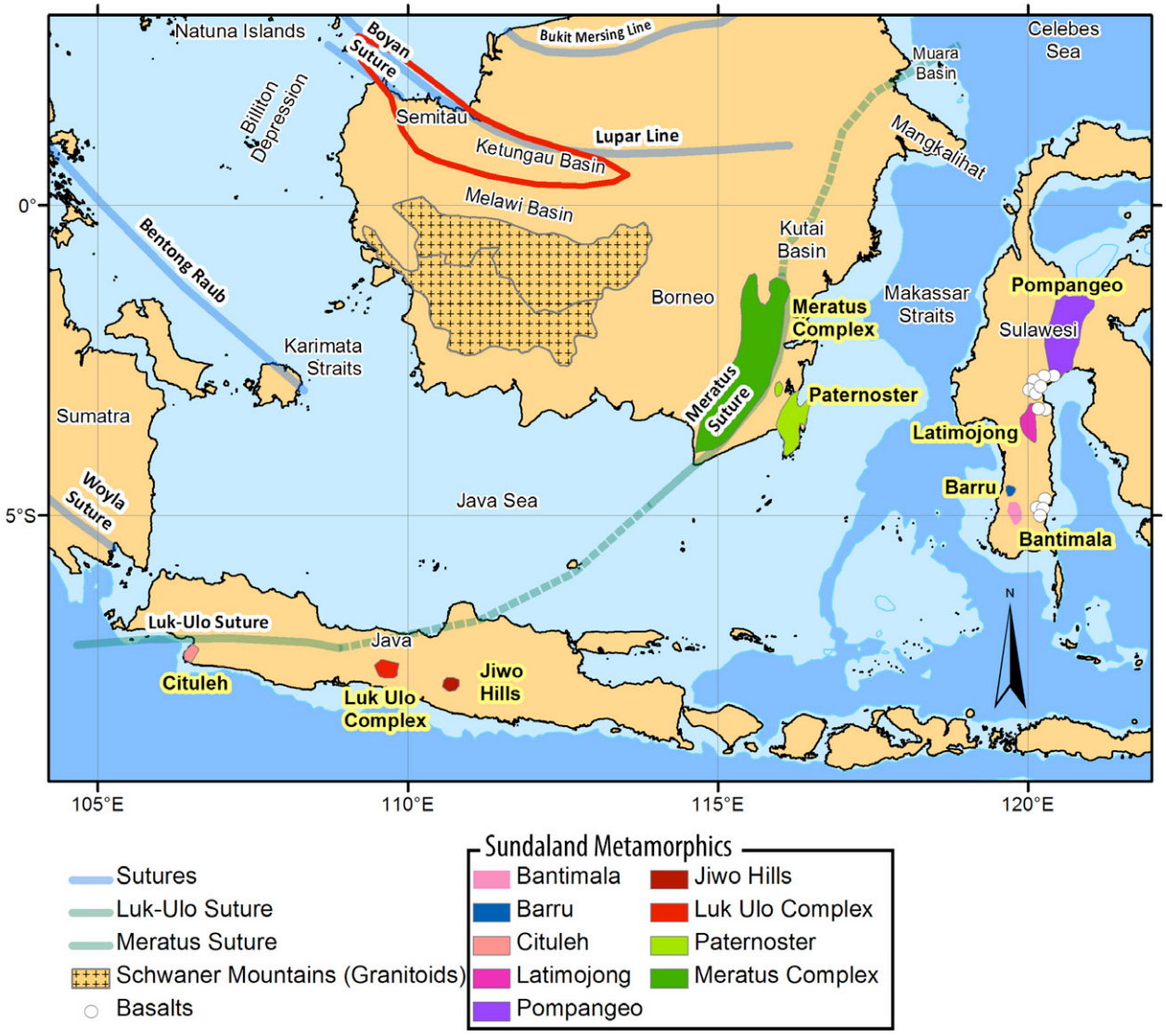

Figure A1. The accretion history of Sundaland is contained within metamorphic belts (Wakita, 2000) that span east Java and Borneo across the Luk-Ulo and Meratus sutures. These metamorphic belts record the onset of peak metamorphism at ~115 Ma (Parkinson et al., 1998), with final suturing to the Sundaland core by ~80 Ma (Clements and Hall, 2011; Wakita, 2000).

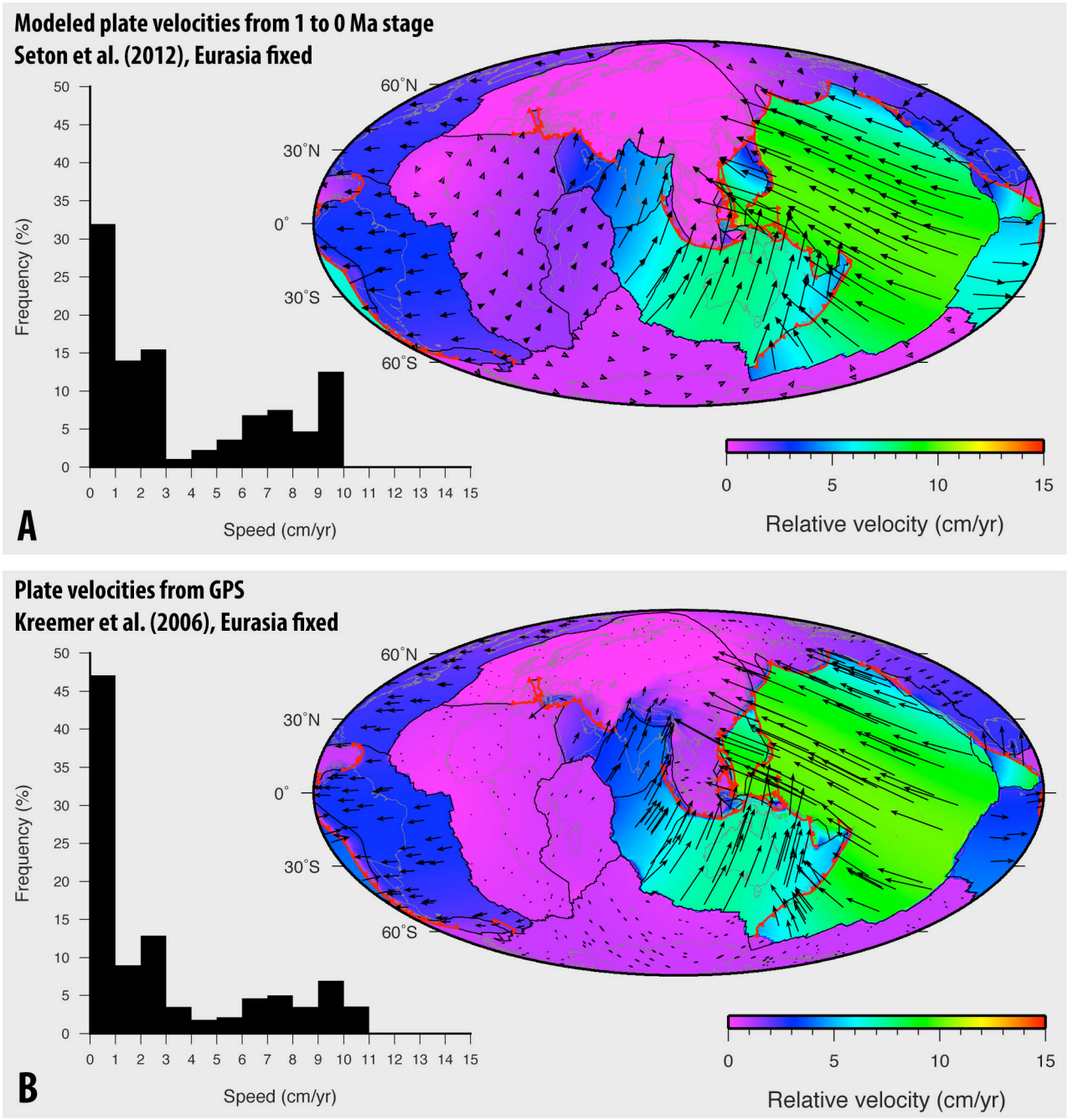

Figure A2. Present-day velocities predicted by the stage rotations from 1 to 0 Ma from our model [top] compared to the plate velocities derived from GPS stations in a Eurasia-fixed reference frame. The velocity azimuths and magnitudes are very similar, with differences largely confined to deforming continental regions.

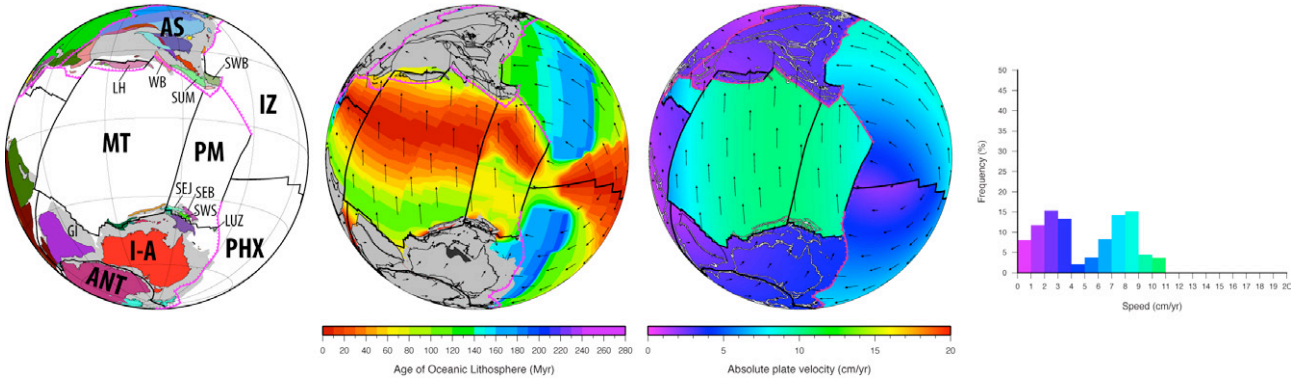

Figure A3. Plate reconstruction at 155 Ma depicting the development of a triple junction along the northern Gondwana margin initiating rifting of the Southeast Java (SEJ), Southeast Borneo (SEB) and Southwest Sulawesi (SWS) along the northern margin of the Indo-Australian Plate (I-A). Continental regions are grey, present-day coastlines are thin black lines, transforms/mid-oceanic ridges (thick black lines), subduction zones (teethed magenta lines) and large igneous provinces (dark grey) are reconstructed in the centre. Absolute plate velocity distributions [right] indicate that the MesoTethys (MT) and Proto Molucca (PM) plates have a higher northward velocity resulting from northward slab-pull from north-dipping subduction beneath Eurasia, including Lhasa (LH), West Burma (WB), Sumatra (SUM) and the Southwest Borneo (SWB) core. A frequency histogram [right] depicts the distribution of modelled absolute plate velocity magnitudes at this time.

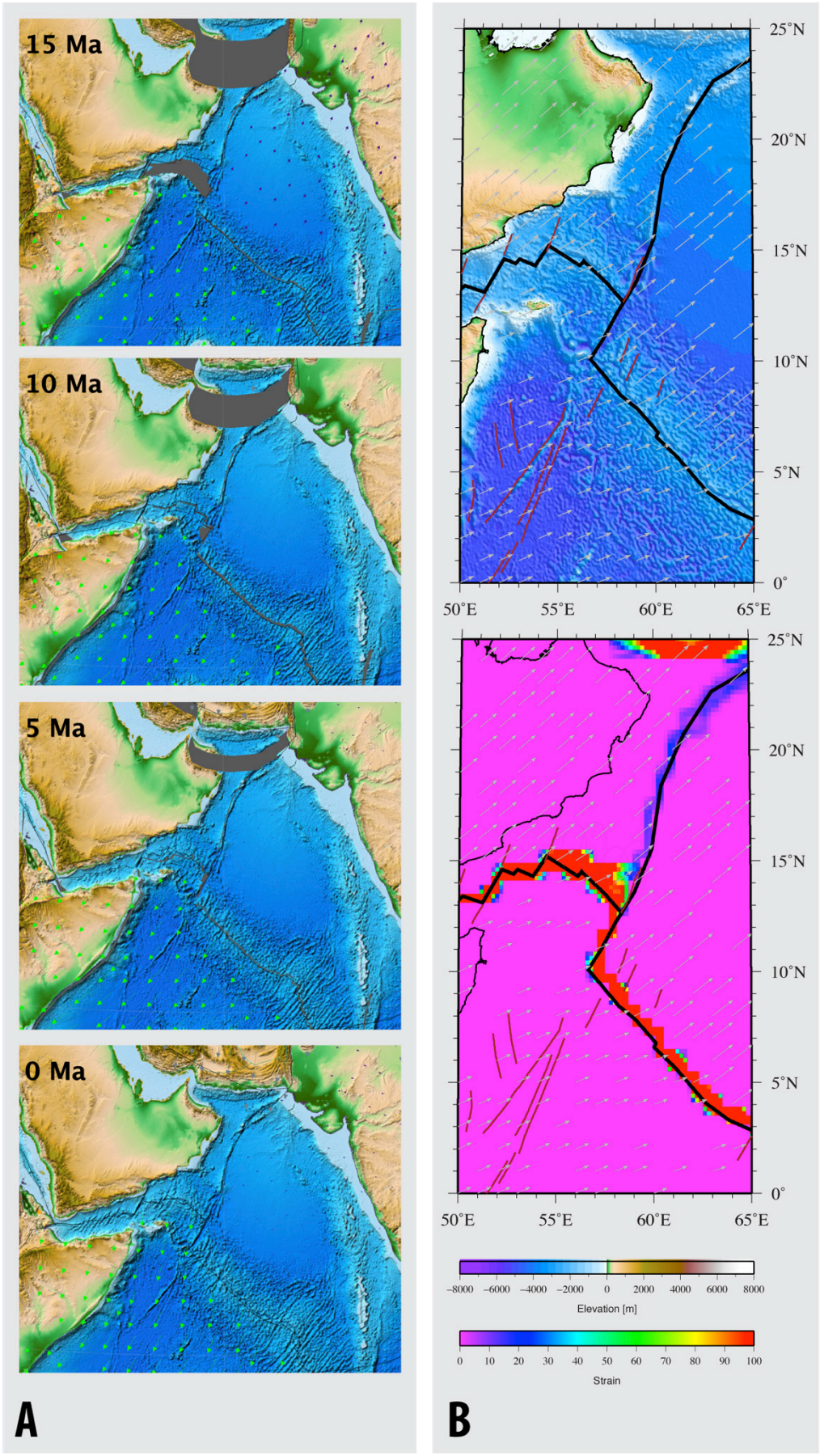

Figure A4. a) Plate reconstructions in an Arabia-fixed frame, with plate boundaries (black) and coloured arrows representing relative plate motions highlighting slightly oblique motions along the

Owen Fracture Zone since 15 Ma, compared to b) Present-day plate configurations with second invariant of strain rate and no-net rotation plate velocities (grey arrows) from Kreemer et al. (2003) highlighting deformation localised along the Owen Fracture Zone, which is accommodating oblique motion with components of strike-slip and extension. We propose that the eastern MesoTethyan-Junction transform became oblique to accommodate extension to become the third arm of a triple junction near the Bird's Head on New Guinea at ~155 Ma. Fracture zones are from Matthews et al. (2011) and present-day topography from Amante et al. (2009) is reconstructed in GPlates.

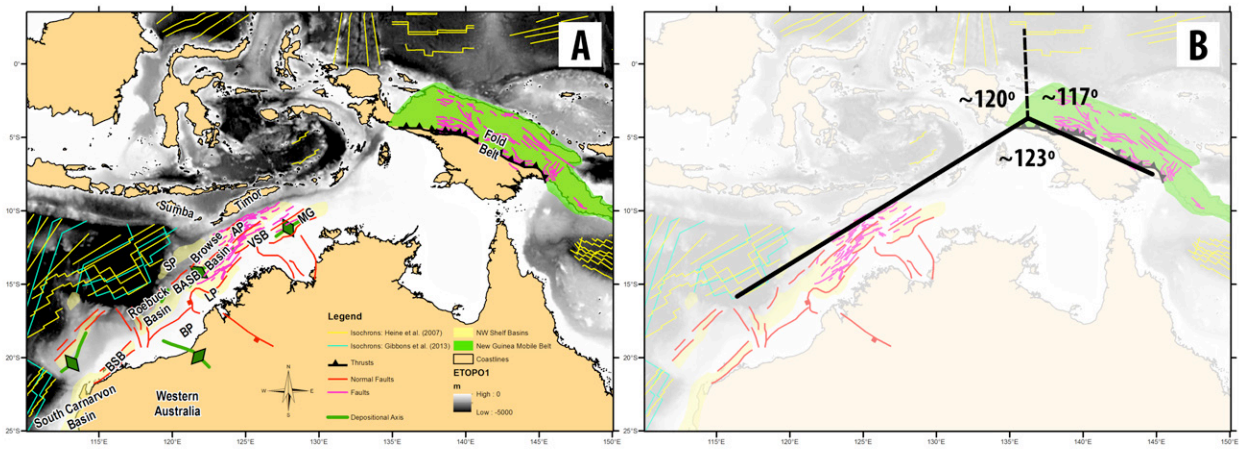

Figure A5. A) The tectonic structural fabric of the NW Australian shelf, inherited from latest Jurassic-Early Cretaceous rifting and seafloor spreading is highlighted by faults, basin depositional axes and seafloor age trends. Similarly, the outline of the stable part of New Guinea is delimited by the Mobile and Thrust belts, with structures highlighted by regional faulting. Faults and basins on the NW Shelf were digitized from Keep and Harrowfield (2005), and on New Guinea from Cooper and Taylor (1987), Abers and McCaffrey (1988), and Simandjuntak and Barber (1996). Seafloor spreading isochrons on the NW Shelf are from Heine and Müller (2005) and from Gibbons et al. (2012; 2013). B) The intersection between these fabrics produces a ~123° angle between the NW Shelf and the New Guinea margin in the latest Jurassic. Seafloor spreading initiated on both margins contemporaneously, with a slight lag likely on the NW Shelf due to the westward propagation of seafloor spreading. To accommodate this, a triple junction may be required, with the third arm likely having a ~N-S orientation in present-day co-ordinates.

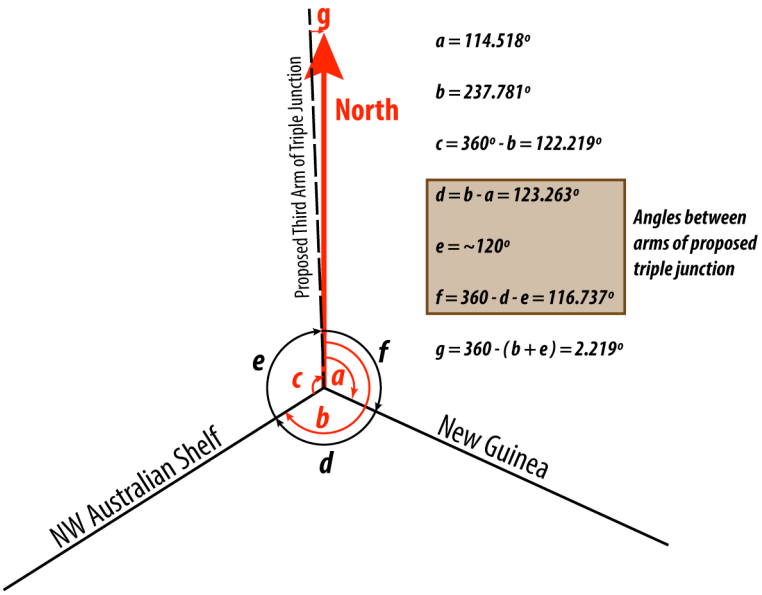

Figure A6. The geometry of the proposed triple junction between the NW Australian Shelf and the New Guinea margin is derived from the structural fabric on these margins (see Fig. A4). The angle between the NW Australian and New Guinea margins is calculated to be ~123° (*d*), and the third arm of the proposed triple junction is derived by adding 120° (*e*), which is the approximate angle required.

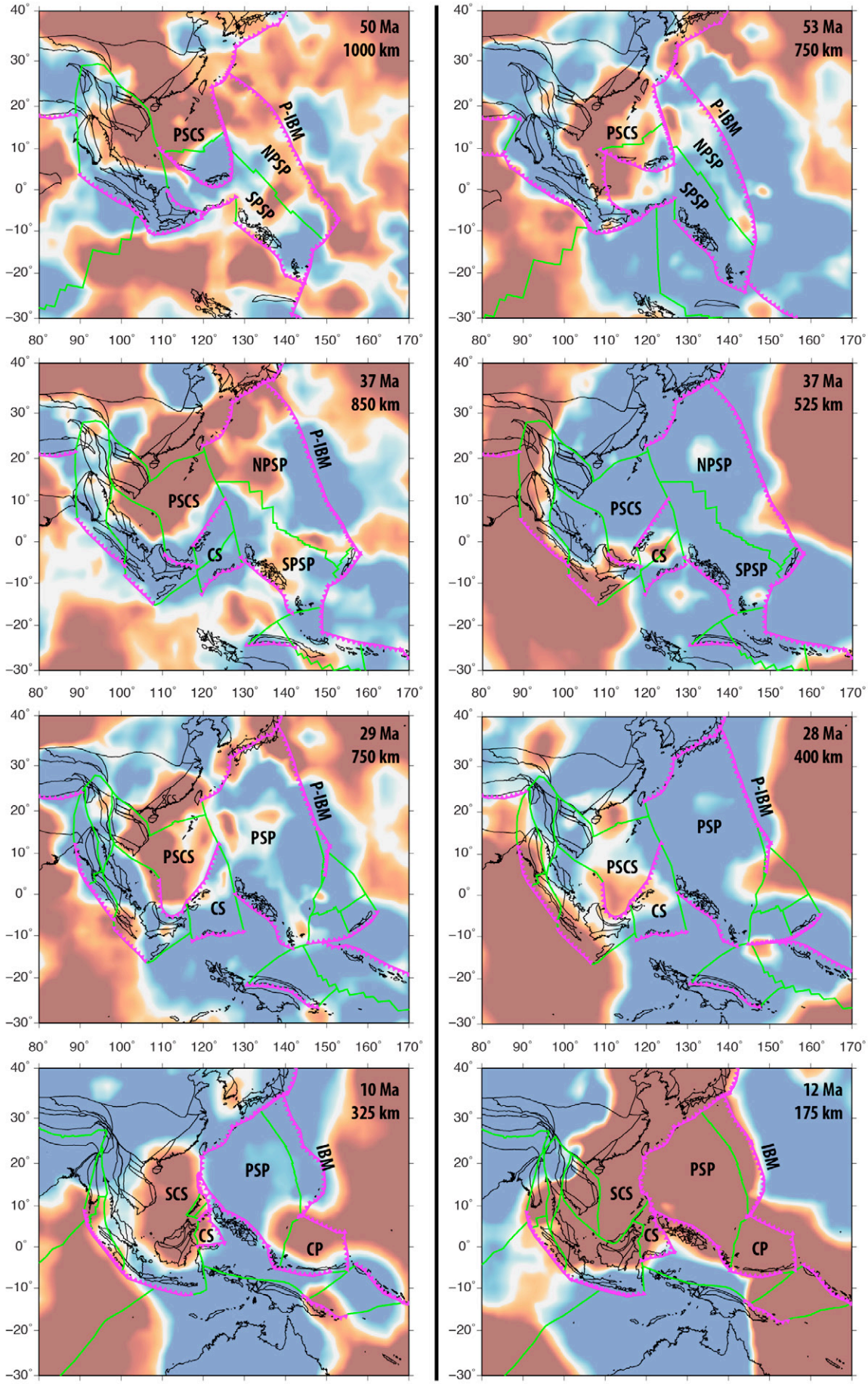
50 Ma
1000 km
PSCS
P-IBM
NPSP
SPSP
53 Ma
750 km
PSCS
P-IBM
NPSP
SPSP
37 Ma
850 km
NPSP
P-IBM
PSCS
CS
SPSP
37 Ma
525 km
NPSP
PSCS
CS
SPSP
29 Ma
750 km
P-IBM
PSP
PSCS
CS
28 Ma
400 km
P-IBM
PSP
PSCS
CS
10 Ma
325 km
IBM
PSP
SCS
CS
CP
12 Ma
175 km
IBM
PSP
SCS
CS
CP
Sinking Rate Scenario 1
Sinking Rate Scenario 2
−0.5 −0.4 −0.3 −0.2 −0.1 0.0 0.1 0.2 0.3 0.4 0.5
Velocity Perturbation (%)

Figure A7. Plate reconstructions superimposed on age-coded depth slices of GyPSuM S-wave seismic tomography (Simmons et al., 2010) with two end-member sinking rate scenarios. Scenario 1 applies a 3 and 1.2 cm/yr sinking rate of slabs in the upper and lower mantle, respectively, following Zahirovic et al. (2012). Scenario 2 applies a whole-mantle slab sinking rate of 1.4 cm/yr as a low sinking rate end-member. Reconstructed block outlines (black) and plate boundaries (MORs/Transforms = green, Subduction Zones = magenta)are plotted for reference. CP = Caroline Plate, CS = Celebes Sea, SCS = South China Sea, PSCS = Proto South China Sea, NPSP = North Philippine Sea Plate, SPSP = South Philippine Sea Plate, (P-) IBM = (Proto-) Izu-Bonin-Mariana Arc.

Appendix B

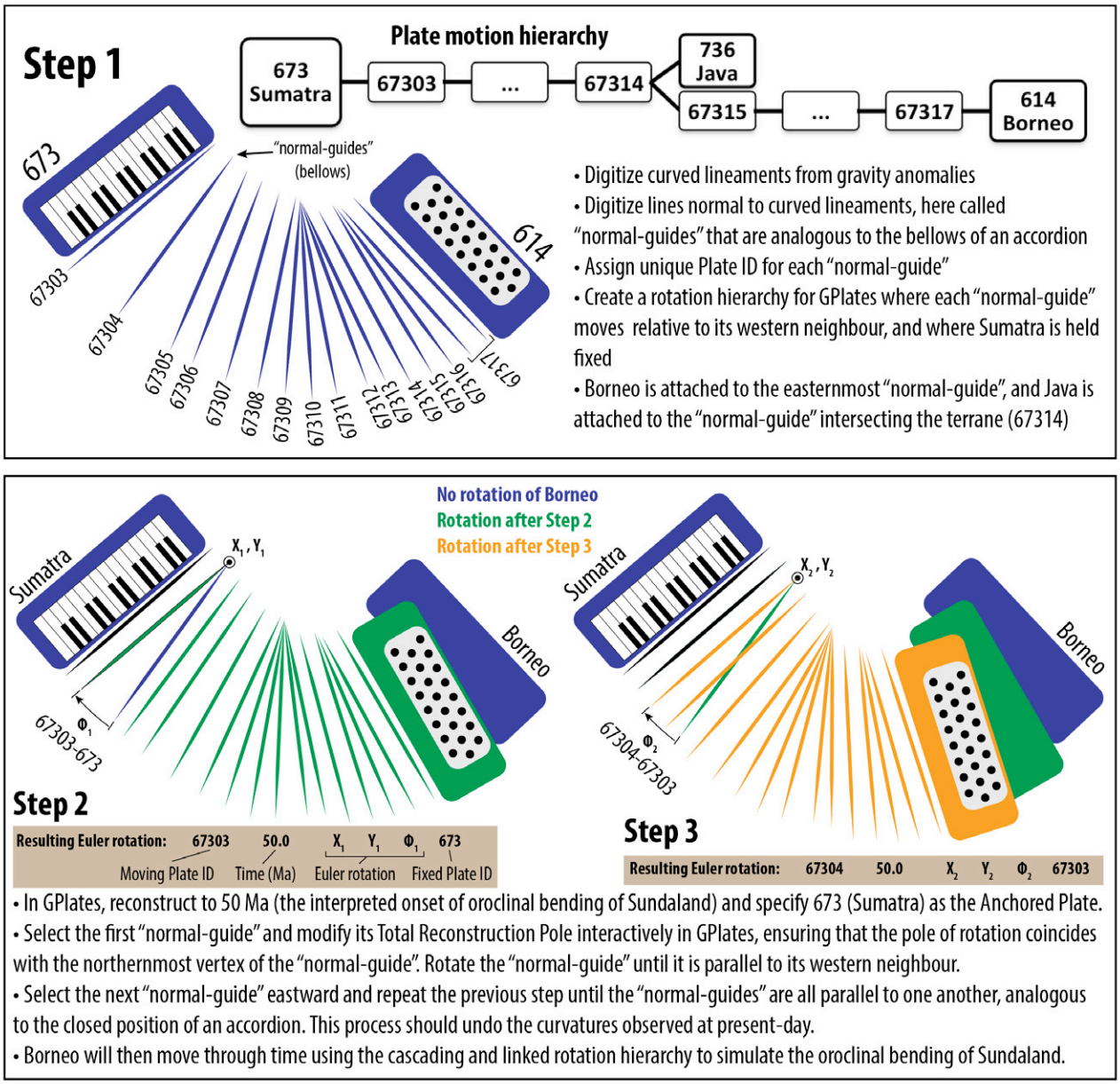

Figure B1. Method describing the process of deriving Euler rotations to simulate the oroclinal bending of Sundaland, with Sumatra held fixed and Borneo moving through a cascading plate motion hierarchy (Step 1). In this simplification of oroclinal bending of Sundaland, we apply the analogues of an accordion where the present-day curved lineaments on Sundaland represent an "open" position of the accordion. Lines normal to the curved lineaments are analogous to the vertical bellows of an accordion, and are parallel to one another when there is no curvature of the accordion. In the same way, these "normal-guides" are rotated using *GPlates* to reverse oroclinal bending by returning the "normal-guides" (i.e. bellows) into a parallel position (Steps 2 and 3). The age of oroclinal bending and cessation can be easily modified following the example in the provided global rotation file (see Appendix C). The finite Euler rotation at the beginning of the oroclinal bending (i.e. 50 Ma) will not change if the age of oroclinal bending is modified to another

time (i.e. 80 Ma), as the pre-oroclinal bending geometry derived using our method is time-independent – as long as all the ages are changed consistently in the plate motion hierarchy created in Step 1. In our preferred model, we partition the oroclinal bending of Sundaland between 50 and 10 Ma, with 50° CCW rotation confined to the 25 to 10 Ma time interval based on paleomagnetic constraints (Fuller et al., 1999).

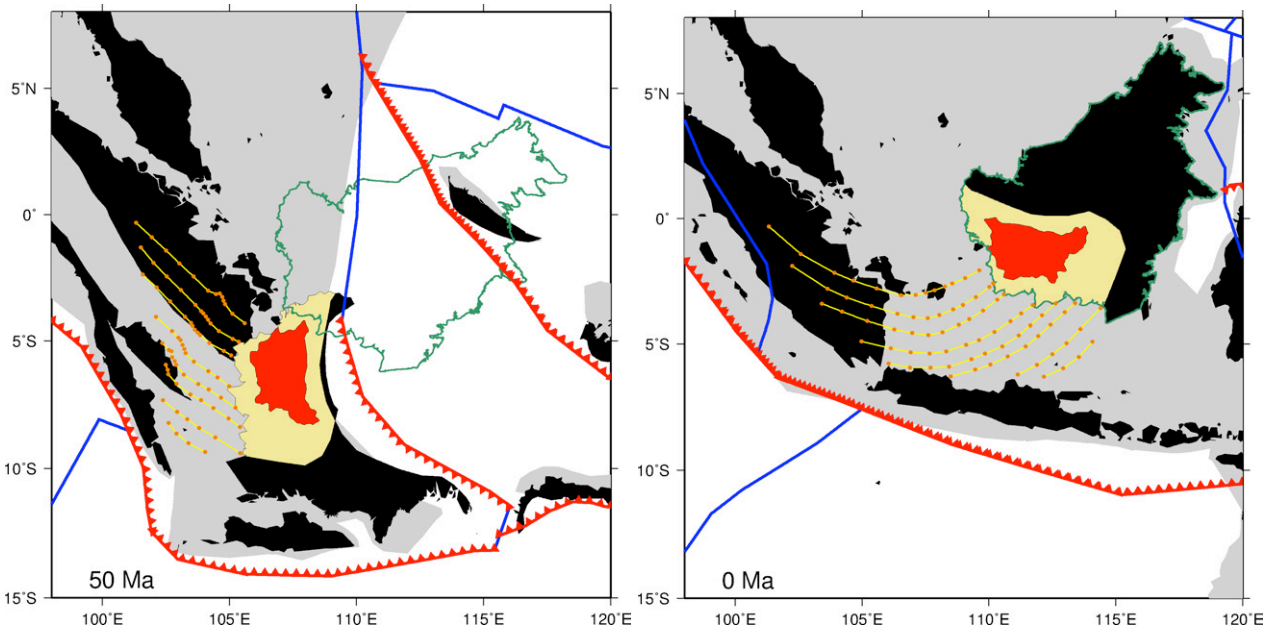

Figure B2. The position of Borneo restored at 50 Ma [left] using the preferred oroclinal bending model for Sundaland, where the curvatures (yellow lines) are straightened and the "normal-guides" (orange points) are parallel to one another like the bellows of a close musical accordion, and at present-day are curved [right] as a result of the oroclinal bending. The plate boundary configuration (MORs/Transforms = blue, Subduction Zones = red), reconstructed present-day coastlines (filled black) and reconstruction of Borneo from Lee and Lawver (1995; green) is plotted for reference in a Sumatra-fixed reference frame.

Table B1. Equivalent finite rotations of Borneo relative to Sumatra in 1 Myr intervals derived from the preferred oroclinal bending model of Sundaland, assuming oroclinal bending initiated at 50 Ma contemporaneous to the onset of basin rifting in the Java Sea, and complete by 10 Ma. Up to ~50° CCW rotation of Borneo is accommodated between 25 and 10 Ma based on paleomagnetic constraints (Fuller et al., 1999).

Age (Ma)	Lat	Lon	Angle
0.0	0.00	0.00	0.00
10.0	0.00	0.00	0.00
11.0	-0.38	106.96	-3.33
12.0	-0.41	106.94	-6.67
13.0	-0.43	106.91	-10.00
14.0	-0.46	106.88	-13.34
15.0	-0.48	106.86	-16.67
16.0	-0.51	106.83	-20.01
17.0	-0.53	106.80	-23.34
18.0	-0.56	106.77	-26.68
19.0	-0.58	106.74	-30.01
20.0	-0.61	106.72	-33.35
21.0	-0.63	106.69	-36.68
22.0	-0.66	106.66	-40.02
23.0	-0.68	106.63	-43.35
24.0	-0.71	106.60	-46.69
25.0	-0.73	106.57	-50.02
26.0	-0.74	106.56	-51.13
27.0	-0.75	106.55	-52.24
28.0	-0.76	106.54	-53.35
29.0	-0.77	106.53	-54.47
30.0	-0.78	106.52	-55.58
31.0	-0.78	106.51	-56.69
32.0	-0.79	106.50	-57.80
33.0	-0.80	106.49	-58.91
34.0	-0.81	106.48	-60.02
35.0	-0.82	106.47	-61.13
36.0	-0.83	106.46	-62.24
37.0	-0.84	106.45	-63.35
38.0	-0.85	106.44	-64.46
39.0	-0.85	106.43	-65.57
40.0	-0.86	106.42	-66.69
41.0	-0.87	106.41	-67.80
42.0	-0.88	106.40	-68.91
43.0	-0.89	106.39	-70.02
44.0	-0.90	106.38	-71.13
45.0	-0.91	106.37	-72.24
46.0	-0.92	106.36	-73.35
47.0	-0.92	106.35	-74.46
48.0	-0.93	106.34	-75.57

49.0	-0.94	106.33	-76.68
50.0	-0.95	106.32	-77.79

Table B2. Finite Euler rotation parameters for the normal-guides that define the oroclinal bending model preferred in this study. The first column represents the Plate ID of the "normal-guides" that are rotated in GPlates to undo oroclinal bending, and their rotation hierarchy can be followed through the 'Moving Plate ID' and 'Relative Plate ID' plate circuits (see Fig. B1).

Moving Plate ID	Age (Ma)	Lat	Lon	Angle	Relative Plate ID	
67303	0.0	0.00	0.00	0.00	673	Relative to Sumatra
67303	10.0	0.00	0.00	0.00	673	Relative to Sumatra
67303	25.0	2.10	104.94	-7.21	673	Relative to Sumatra
67303	50.0	-2.10	-75.06	11.21	673	Relative to Sumatra
67303	300.0	-2.10	-75.06	11.21	673	Relative to Sumatra
67304	0.0	0.00	0.00	0.00	67303	
67304	10.0	0.00	0.00	0.00	67303	
67304	25.0	1.55	105.43	-6.97	67303	
67304	50.0	-1.55	-74.57	10.84	67303	
67304	300.0	-1.55	-74.57	10.84	67303	
67305	0.0	0.00	0.00	0.00	67304	
67305	10.0	0.00	0.00	0.00	67304	
67305	25.0	0.89	106.38	-0.68	67304	
67305	50.0	-0.89	-73.62	1.06	67304	
67305	300.0	-0.89	-73.62	1.06	67304	
67306	0.0	0.00	0.00	0.00	67305	
67306	10.0	0.00	0.00	0.00	67305	
67306	25.0	0.31	106.24	-2.47	67305	
67306	50.0	-0.31	-73.76	3.84	67305	
67306	300.0	-0.31	-73.76	3.84	67305	
67307	0.0	0.00	0.00	0.00	67306	
67307	10.0	0.00	0.00	0.00	67306	
67307	25.0	0.10	-73.06	2.39	67306	
67307	50.0	0.10	-73.06	3.72	67306	
67307	300.0	0.10	-73.06	3.72	67306	
67308	0.0	0.00	0.00	0.00	67307	
67308	10.0	0.00	0.00	0.00	67307	
67308	25.0	0.14	-72.58	3.05	67307	
67308	50.0	0.14	-72.58	4.75	67307	
67308	300.0	0.14	-72.58	4.75	67307	
67309	0.0	0.00	0.00	0.00	67308	
67309	10.0	0.00	0.00	0.00	67308	
67309	25.0	0.78	-72.50	4.96	67308	
67309	50.0	0.78	-72.50	7.72	67308	
67309	300.0	0.78	-72.50	7.72	67308	
67310	0.0	0.00	0.00	0.00	67309	

67310	10.0	0.00	0.00	0.00	67309
67310	25.0	1.42	-73.41	4.37	67309
67310	50.0	1.42	-73.41	6.80	67309
67310	300.0	1.42	-73.41	6.80	67309
67311	0.0	0.00	0.00	0.00	67310
67311	10.0	0.00	0.00	0.00	67310
67311	25.0	1.03	-73.26	5.41	67310
67311	50.0	1.03	-73.26	8.41	67310
67311	300.0	1.03	-73.26	8.41	67310
67312	0.0	0.00	0.00	0.00	67311
67312	10.0	0.00	0.00	0.00	67311
67312	25.0	1.28	-72.98	3.45	67311
67312	50.0	1.28	-72.98	5.36	67311
67312	300.0	1.28	-72.98	5.36	67311
67313	0.0	0.00	0.00	0.00	67312
67313	10.0	0.00	0.00	0.00	67312
67313	25.0	1.62	-73.34	1.95	67312
67313	50.0	1.62	-73.34	3.03	67312
67313	300.0	1.62	-73.34	3.03	67312
67314	0.0	0.00	0.00	0.00	67313
67314	10.0	0.00	0.00	0.00	67313
67314	25.0	0.67	-71.18	0.81	67313
67314	50.0	0.67	-71.18	1.26	67313
67314	300.0	0.67	-71.18	1.26	67313
67315	0.0	0.00	0.00	0.00	67314
67315	10.0	0.00	0.00	0.00	67314
67315	25.0	3.14	-69.41	3.15	67314
67315	50.0	3.14	-69.41	4.90	67314
67315	300.0	3.14	-69.41	4.90	67314
67316	0.0	0.00	0.00	0.00	67315
67316	10.0	0.00	0.00	0.00	67315
67316	25.0	3.53	-68.53	2.24	67315
67316	50.0	3.53	-68.53	3.48	67315
67316	300.0	3.53	-68.53	3.48	67315
67317	0.0	0.00	0.00	0.00	67316
67317	10.0	0.00	0.00	0.00	67316
67317	25.0	3.01	-67.73	0.96	67316
67317	50.0	3.01	-67.73	1.49	67316
67317	300.0	3.01	-67.73	1.49	67316
614	0.0	0.00	0.00	0.00	67317
614	300.0	0.00	0.00	0.00	67317

Borneo relative to curved lineaments

Borneo relative to curved lineaments

Table B3. Finite Euler rotations of the Southwest Borneo Core relative to Eurasia derived from the oroclinal bending model in 5 Myr intervals. An additional amount of rotation of Borneo results from large offset strike-slip faults in Southeast Asia (e.g. Sagaing, Three Pagodas, Ranong, etc.).

Age (Ma)	Lat	Lon	Angle
0.0	0.00	0.00	0.00
5.0	7.07	112.11	-0.003
10.0	5.91	109.99	-0.01
15.0	0.56	106.34	-17.36
20.0	0.36	106.03	-34.62
25.0	0.01	106.53	-52.29
30.0	0.65	106.92	-59.63
35.0	-0.04	107.79	-58.38
40.0	-0.75	108.79	-56.97
45.0	-1.28	109.61	-56.97
50.0	-1.19	109.35	-62.45
55.0	-1.21	109.38	-62.38
60.0	-1.10	109.29	-63.95
65.0	-0.97	109.17	-65.93
70.0	-0.84	109.05	-67.91
75.0	-0.80	109.03	-68.66
80.0	-0.82	109.06	-68.60
85.0	-0.84	109.10	-68.53
90.0	-0.76	108.89	-69.78
95.0	-0.62	108.53	-71.89
100.0	-0.50	108.19	-74.01
105.0	-0.37	107.87	-76.13
110.0	-0.25	107.57	-78.25
115.0	-0.14	107.27	-80.37
120.0	-0.15	107.30	-80.31
125.0	-0.16	107.33	-80.24
130.0	-0.17	107.36	-80.17
135.0	-0.18	107.38	-80.13
140.0	-0.18	107.38	-80.13
145.0	-0.18	107.38	-80.13
150.0	-0.18	107.38	-80.13
155.0	-0.04	106.24	-81.50

Table B4. Equivalent finite rotations of Borneo relative to Sumatra in 5 Myr intervals assuming that oroclinal bending of Sundaland was partitioned equally between 80 and 13 Ma, which we propose as an alternative model. However, our preferred model (implemented in the global plate motion model) is presented in Table B1, and partitions the oroclinal bending between 50 and 10 Ma instead. The onset of oroclinal bending may have occurred as early as 80 Ma resulting from the accretion of Gondwana-derived continental blocks to the Borneo core, and may have ceased by ~13 Ma following the onset of regional basin inversions on the Sunda Shelf. The GPlates rotation file allows users to easily change these timings so that alternative models can be tested in the future to simulate crustal stretching of the Sunda Shelf that can be validated using constraints from seismic refraction and gravity inversion studies.

Age (Ma)	Lat	Lon	Angle
0.0	0.00	0.00	0.00
13.0	0.00	0.00	0.00
15.0	-0.37	106.97	-2.32
20.0	-0.42	106.92	-8.13
25.0	-0.46	106.88	-13.93
30.0	-0.50	106.83	-19.74
35.0	-0.55	106.78	-25.55
40.0	-0.59	106.73	-31.35
45.0	-0.63	106.68	-37.16
50.0	-0.68	106.63	-42.96
55.0	-0.72	106.58	-48.77
60.0	-0.77	106.53	-54.57
65.0	-0.81	106.48	-60.38
70.0	-0.86	106.43	-66.18
75.0	-0.90	106.37	-71.99
80.0	-0.95	106.32	-77.79

Appendix C

GPlates model files

We include a number of digital files in order to make our work replicable and testable. We provide the plate motion model used in our reconstructions; including a GPlates rotation file and present-day coastlines. Resolved topologies that result from the intersection of global plate boundaries are also bundled at 1 Myr intervals. Due to file-size restrictions, we upload the full zipped folder of the resolved topologies to our website[1] and only provide the Shapefile ".shp" versions in this Supplement. We also include the reconstructed line geometries of Transforms and Mid-oceanic Ridges (topology_ridge_transform_boundaries_${Age}.00Ma.shp) and Subduction Zones (topology_subduction_boundaries_${Age}.00Ma.shp), where ${Age} is the geological time in million years before present. To aid in the plotting of subduction polarities, we also include two files representing global subduction zones for each 1 Myr timestep:

topology_subduction_boundaries_sL_${Age}.00Ma.shp
topology_subduction_boundaries_sR_${Age}.00Ma.shp

Where "sR" contains subduction zones that have subduction occurring to the right along the line in the direction it was digitized (i.e. the slab is to the right of the line), and vice versa for "sL". In GMT, the PSXY command that plots weather fronts can be used to represent this symbology (i.e. "teeth"). An example GMT4 (http://www.soest.hawaii.edu/gmt/) plotting script called "Zahirovic_2014_GMT_Plot.sh" and the GMT ".xy" version of the topologies with subduction symbology is available from our website due to filesize limitations for Supplementary Material.

To manipulate and visualise the plate motion model, you will need to download GPlates (recommended version 1.3 or later, www.gplates.org). To load the model, open GPlates, go to File > Open Feature Collection, navigate to the unzipped supplementary material and select the three files in the folder:

1_PlateModel/1_GPlatesBundle/
Zahirovic_etal_SoutheastAsia_Coastlines.gpmlz
Zahirovic_etal_SoutheastAsia_StaticPolygons.gpmlz
Zahirovic_etal_SoutheastAsia_EarthByte_2014.rot

[1] http://www.earthbyte.org/Resources/Zahirovic_etal_SoutheastAsia.html

The GPMLZ files are compressed GPlates-specific geometry files that contain the cookie-cut coastlines (by Plate ID) and the cookie-cutting age-coded static polygons for the continents and oceans. To obtain Shapefiles, OGR-GMT or GMT xy versions of any geometry layer in GPlates, you can go to File > Manage Feature Collection, click on 'Save As' and choose the output file type.

Animations

Animations in MPEG-4 format are provided, including:

Zahirovic_etal_Asia_AgeGrid.mp4 – Orthographic hemispherical animation with seafloor age-grids and plate boundaries

Zahirovic_etal_Asia_BasinsVolcanics.mp4 – Mercator animation with seafloor age-grids, plate boundaries, volcanics and basin tectonic regime

Zahirovic_etal_Asia_ColourCoded.mp4 – Orthographic hemispherical animation with colour-coded tectonic elements, plate boundaries and plate velocity vectors

Zahirovic_etal_Asia_Velocities.mp4 – Orthographic hemispherical animation with plate velocity vectors, velocity grids and plate boundaries

Zahirovic_etal_Asia_WGM_Bouguer_FreeAir.avi – Profiles crossing the Billiton Depression and the Luk-Ulo and Meratus Suture on the Sunda Shelf with a comparison of Bouguer and Free-air gravity anomalies along each profile.

Zahirovic_etal_Asia_WGM_Bouguer_Bathymetry.avi – Profiles crossing the Billiton Depression and the Luk-Ulo and Meratus Suture on the Sunda Shelf with a comparison of Bouguer gravity anomalies and GMRT bathymetry.

Additional animations, including animations in QuickTime format are available from:
http://www.earthbyte.org/Resources/Zahirovic_etal_SoutheastAsia.html

> **Note:** **If animations fail to work, try installing and using VideoLAN Player (open-source and cross-platform) from http://www.videolan.org/**

Digitized regional features

Many digitized and georeferenced regional geological features including ophiolites, suture zones, metamorphics, volcanics and age-coded basins are provided in folder "3_DigitizedFeatures". They are all in Shapefile format, and the age-coded basins have Plate IDs and time spans associated with

them for use in GPlates. If you use any of these files, please make sure you also cite the original source, which can be found in the figure captions and tables in the main text and Appendix.

Volcanics: Soeria-Atmadja, R., Noeradi, D., and Priadi, B.: Cenozoic magmatism in Kalimantan and its related geodynamic evolution, Journal of Asian Earth Sciences, 17, 1, 25-45, 1999.

Basins: Doust, H., and Sumner, H. S.: Petroleum systems in rift basins–a collective approach in Southeast Asian basins, Petroleum Geoscience, 13, 2, 127-144, 2007.

Support

If any files do not work, or more help is required, please e-mail the corresponding author:
Sabin Zahirovic – sabin.zahirovic@sydney.edu.au

References

Abers, G., and McCaffrey, R.: Active deformation in the New Guinea fold-and-thrust belt: Seismological evidence for strike-slip faulting and basement-involved thrusting, Journal of Geophysical Research: Solid Earth (1978–2012), 93, B11, 13332-1335410.1029/JB093iB11p13332, 1988.

Amante, C., Eakins, B., and Boulder, C., 2009, ETOPO1 1 arc-minute global relief model: Procedures, data sources and analysis: NOAA Technical Memorandum.

Cooper, P., and Taylor, B.: Seismotectonics of New Guinea: a model for arc reversal following arc-continent collision, Tectonics, 6, 1, 53-6710.1029/TC006i001p00053, 1987.

Heine, C., and Müller, R.: Late Jurassic rifting along the Australian North West Shelf: margin geometry and spreading ridge configuration, Australian Journal of Earth Sciences, 52, 1, 27-3910.1080/08120090500100077, 2005.

Keep, M., and Harrowfield, M.: Basement reactivation and inversion mechanisms in the Timor and Norwegian seas, Geological Society, London, Petroleum Geology Conference series, 6861-87110.1144/0060861, 2005.

Kreemer, C., Holt, W., and Haines, A.: An integrated global model of present-day plate motions and plate boundary deformation, Geophysical Journal International, 154, 1, 8-3410.1046/j.1365-246X.2003.01917.x, 2003.

Matthews, K. J., Müller, R. D., Wessel, P., and Whittaker, J. M.: The tectonic fabric of the ocean basins, Journal of Geophysical Research, 116, B12, B1210910.1029/2011JB008413, 2011.

Simandjuntak, T., and Barber, A.: Contrasting tectonic styles in the Neogene orogenic belts of Indonesia, Geological Society, London, Special Publications, 106, 1, 185-20110.1144/GSL.SP.1996.106.01.12, 1996.
Simmons, N. A., Forte, A. M., Boschi, L., and Grand, S. P.: GyPSuM: A joint tomographic model of mantle density and seismic wave speeds, Journal of Geophysical Research: Solid Earth (1978–2012), 115, B12, 10.1029/2010JB007631, 2010.